Supporting Information

Negative Linear Compressibility in Organic Mineral Ammonium Oxalate Monohydrate with Hydrogen Bonding Wine-rack Motifs

Yuancun Qiao,[a] Kai Wang,[a] Hongsheng Yuan,[a] Ke Yang,[b] and Bo Zou[a,*]

[a]State Key Laboratory of Superhard Materials, Jilin University, Changchun 130012, China

[b]Shanghai Institute of Applied Physics, Chinese Academy of Sciences, Shanghai 201203, China.

High-pressure X-ray Power Diffraction

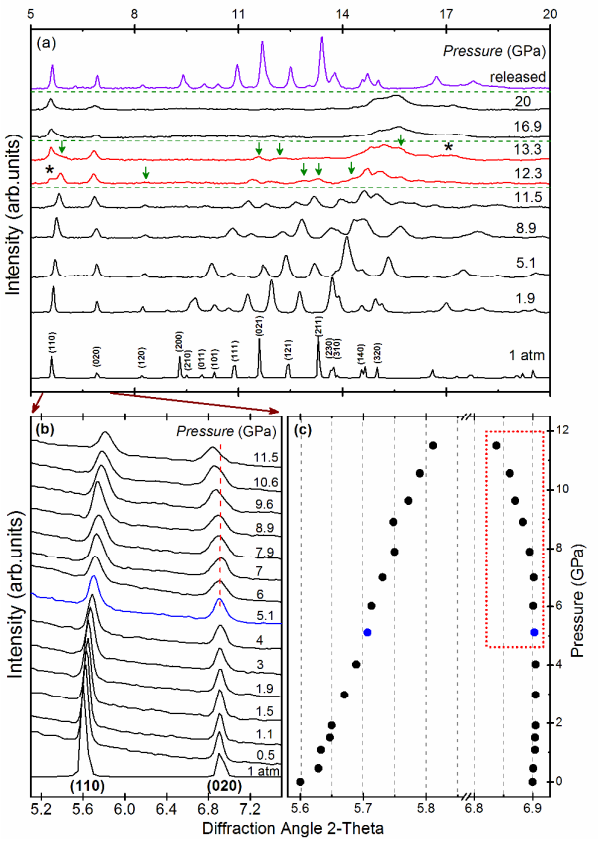

Figure S1. (a) Representative ADXRD patterns at elevated pressures. The phase transition is indicated by asterisk and arrows. (b) Selected (110) and (020) Bragg peaks at variable pressure up to 11.5 GPa. (c) The peak positions of (110) and (020) at various corresponding pressures. The red dashed line and dotted frame highlighted the abnormal behavior of (020) Bragg peak.

The pressure-dependent variations in the XRD patterns are illustrated in Figure S1a. Apart from the pressure-induced typical broadening of the Bragg peaks, all diffraction peaks except the abnormal (020) Bragg peak shift to higher angles with increasing pressure up to 11.5 GPa. At 12.3 GPa, a new narrow peak with a shoulder at the left of Bragg peaks (110) marked with asterisk emerges and its intensity gradually strengthens with pressure up to 15.1 GPa. Meanwhile, most of Bragg peaks marked with green downward arrows becomes weaker and eventually disappeared at higher pressures. From the clear discontinuities in high-pressure XRD patterns, we

can deduce that there is a phase transition in ammonium oxalate monohydrate over the pressure range of 12.3-13.3 GPa. Furthermore, the XRD patterns released to ambient pressure reveal that the high-pressure phase completely returned to its original crystal structure. Figure S1b shows the detailed evolution of Bragg peaks (110) and (020) before phase transition. The two peaks show little shifts to higher angles up to 5.1 GPa And then, the (020) Bragg peak, which is directly related to *b*-axis lattice parameter of ammonium oxalate monohydrate, abnormally moves to lower angles with elevated pressure until phase transition.

Lattice Parameters of Ammonium Oxalate Monohydrate

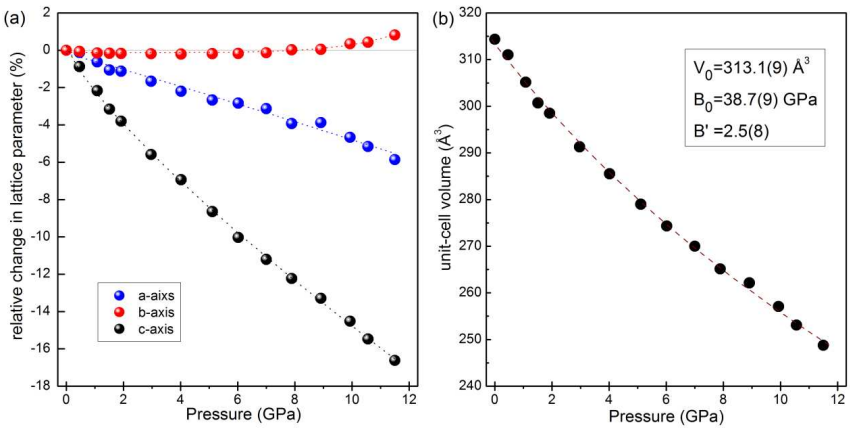

Figure S2. (a) Pressure-dependent relative compression of the three axes, highlighting the extreme anisotropy. (b) Pressure-dependent unit-cell volume. Wine dashed line is 3th-order Birch-Murnaghan equations of state.

Figure S2a shows the relative contraction rate of *a*, *b* and *c*-axis are 5.8 %, -0.9 %, and 16.6 % respectively. The compression is highly anisotropic with the *c*-axis direction being the most compressible. The huge anisotropy in ammonium oxalate monohydrate is an unusual phenomenon which has been discussed by Kuppers in 1972. The large anisotropy of ammonium oxalate monohydrate could be explained by the layer-like packing of the oxalate groups. In addition, the NLC along b-axis also aggravate this anisotropy in ammonium oxalate monohydrate. Figure S2b shows the evolution of unit cell volume as a function of pressure. The volume decreases from 314.4 $Å^3$ at 0 GPa to 248.8 $Å^3$ at 11.5 GPa and the volume totally has a 20.9 % decrease in this pressure range. We suggest that the shrinkage of unit cell volume mostly arises from the compression of *c*-axis. As depicted in the wine curve (Figure S2b), we can see that the third-order Birch−Murnaghan equation of state (B_0'=2.5) describes well with the V (p) data and gives bulk modulus of B_0=38.7 GPa. We note that this value is significantly higher than ordinary organic compounds and even higher than inorganic salt NaCl (B_0=25 GPa). In short, the NLC along *b*-axis aggravates the anisotropy in ammonium oxalate monohydrate and results in a higher bulk modulus value for ammonium oxalate monohydrate.

Table S1. Compounds Showing the NLC Effect

Crystal phase			K_L/TPa^{-1}	Pressure range /GPa	[Ref.]
Inorganic crystal	Simple inorganic crystal	Se	-1.2 [c]	0-7	[1-5]
		$LaNbO_4$	-0.2[210]	0	[1-2, 6]
		NaV_2O_5	-1.6(3)[b]	0-13	[1-2, 7]
		$BAsO_4$	-2[c]	7.5-37	[1-2, 8]
	Metallic cyanide	$Ag_3[Co(CN)_6]$	-75[c]	0-0.19	[9]
			-5[c]	0.19-7.65	
		$KMn[Ag(CN)_2]_3$	-12.0(8)[c]	0-2.2	[10]
		$Zn[Au(CN)_2]_2$	-42(5)[c]	0-1.8	[11]
			-6(3)[c]	1.8-14.2	
		silver(I) tricyanomethanide	-3.5(6)[a]	0-0.615	[12]
			-4.0(6)[c]	0-0.615	
	MOFs	$[NH_4][Zn(HCOO)_3]$	-1.8[c]	0-0.94	[13]
		silver(I) 2-methylimidazolate	-4.32(10)[c]	0-1	[14]
			0.2(3)[c]	0-6.4	
		MIL-53(Al)	-28[b]	0-3	[15]
		NH_2-MIL-53(Al)	-27[b]	0-2	
	Molecular complex	$[Fe(dpp)_2(NCS)_2]\cdot py$	-10.3(20)[a]	0-2.2	[22]
			-41[a]	0-1.82	
		$[(C_6F_5Au)_2(\mu\text{-}1,4\text{-diisocyanoben})]$	-12.57[a]	0-2.41	[16]
			-4.16[a]	0-4.39	
Organic crystal	Methanol monohydrate (160K)		-3.1[a]	0-0.5	[17]
	Ammonium oxalate monohydrate		-2.3(7)[b]	5.1-11.5	This work

Calculated Lattice Parameters of Ammonium Oxalate Monohydrate

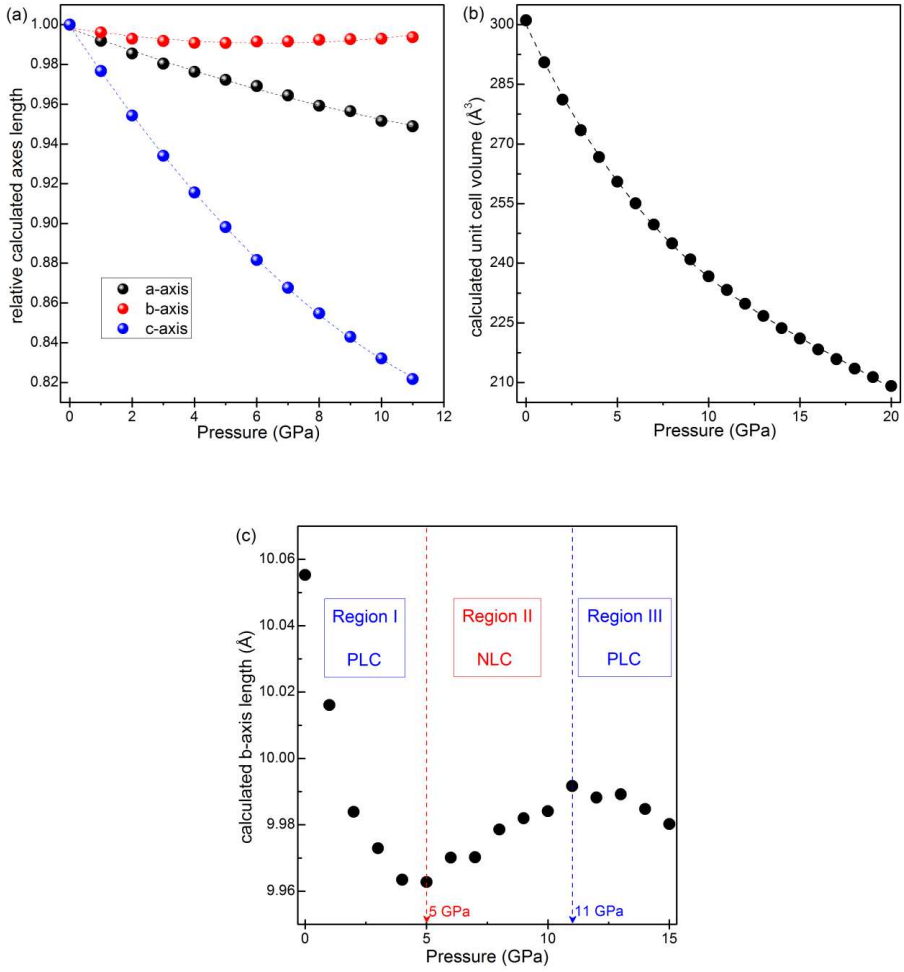

Figure S3. (a). Calculated relative compression of the three axes of ammonium oxalate monohydrate. (b) The calculated unit cell volume at variable pressure. (c) The calculated *b*-axis length with pressure up to 15 GPa.

DFT calculations as an efficient tool have been used to investigated the NLC effects in $KMn[Ag(CN)_2]_3$.[18] In this work, the intriguing high-pressure behaviors of *b*-axis of ammonium oxalate monohydrate are found to be in great agreement with computational data.

Structure Information of Ammonium Oxalate Monohydrate

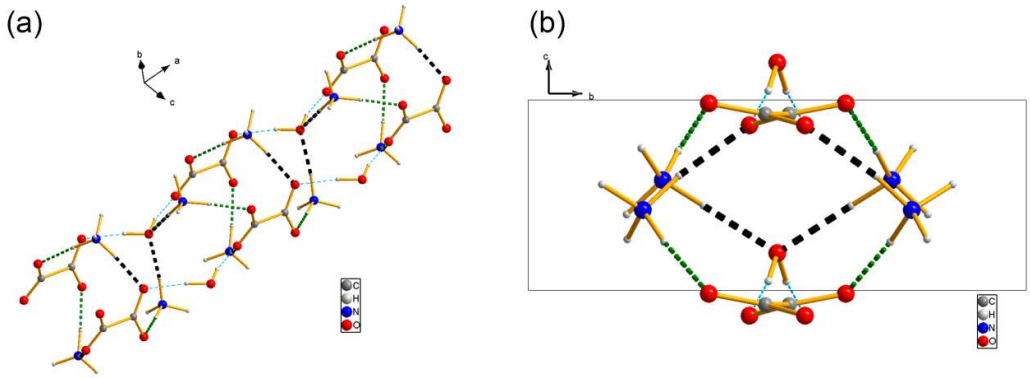

Figure S4 (a) Stereo views of the chain structure and quadrangle helices of N−H···O hydrogen bonds extended along *a*-axis. (b) Plane image viewed along *a*-axis.

High-Pressure Behavior of Several Selected Raman Modes

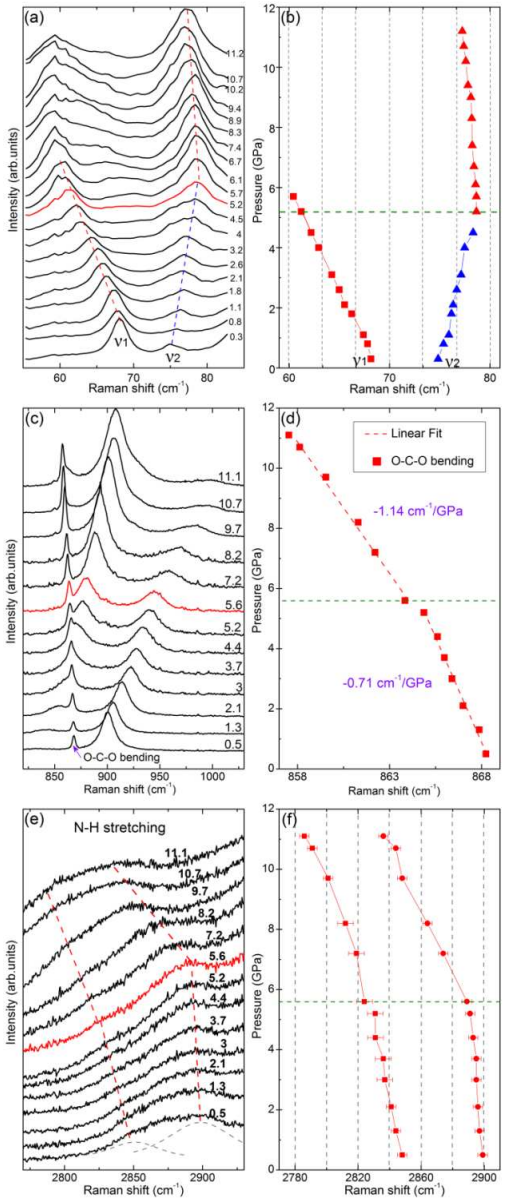

Figure S5. Pressure-dependent external Raman modes (a) and vibrational frequencies (b) in the spectral regions of 55-95 cm^{-1}. Pressure-dependent internal Raman modes (c) and vibrational frequencies (d) in the spectral regions of 800-1050cm^{-1}, and internal Raman modes (e) and vibrational frequencies (f) in the spectral regions of 2750-2950cm^{-1}. All data is collected before phase transition. Green dashed line in panels (b), (d) and (f) highlight the abrupt changes at the critical pressure

In addition to XRD measurements, we carry out high-pressure Raman measurements to have a further understanding of the microscopic mechanism of NLC in ammonium oxalate monohydrate. Generally, vibrational Raman spectroscopy as an efficient tool can probe into the chemical bonding and local structural information.[19-23] The external modes represent intermolecular collective motion in a way. And the external modes in this work involves strong coupling between ammonium cations, oxalate anions and water molecules.[24-25] The detailed evolution of several selected the external and internal Raman spectra as a function of pressure before phase transition is summarized in Figure S5. As shown in Figure S5a, b, the ν_2 mode normally shows a blue shift with increasing pressure at first. Then at a critical pressure 5.2 GPa which corresponds to the start pressure (5.1 GPa) of NLC detected in XRD data, it has a red shift till up to phase transition. Though the NLC in *b*-axis cannot be directly associated with the softening of one of the modes in the external Raman spectrum, the modes displaying red shift appear to be a pre-requisite for NLC systems.[11] Except for the external modes, the internal modes also show an interesting change at a critical pressure (5.6 GPa). As shown in Figure S5c, d, The O-C-O bending mode shows a persistent red shift before phase transition. However, the shift rate after critical pressure is higher than the one before critical pressure. Similarly, we notice that the two N−H stretching modes in the spectral regions of 2750-2950 cm^{-1} highlighted by dash line in Figure S5e, f have a slight red shift up to the critical pressure and then show a vigorous red shift after it. In short, the NLC in ammonium oxalate monohydrate is confirmed by the softening of the external Raman modes and the interesting changes of several selected internal modes at the critical pressure.

Phase Transition of Ammonium Oxalate Monohydrate

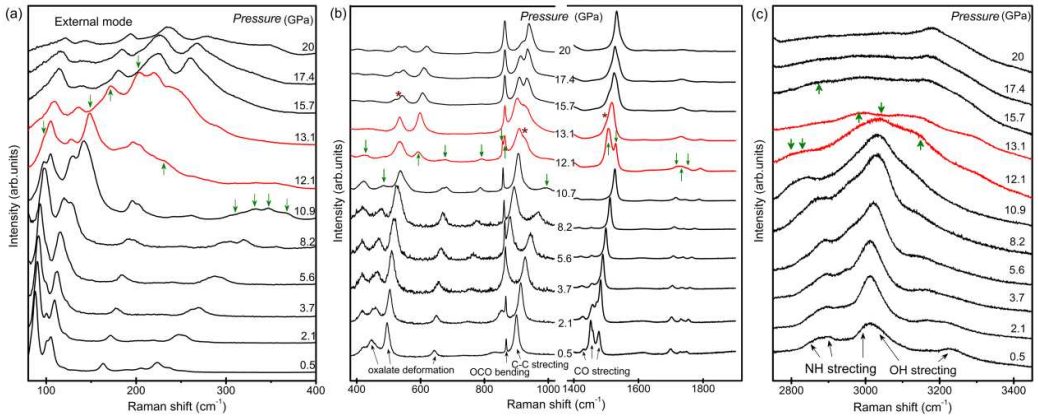

Figure S6. Pressure evolution of Raman spectra in the spectral regions of (a) 80-400, (b) 400-1900, and (c) 2800-3400 cm^{-1} over the pressure range from 0.5 to 20 GPa. The phase transition is indicated by arrows and asterisks.

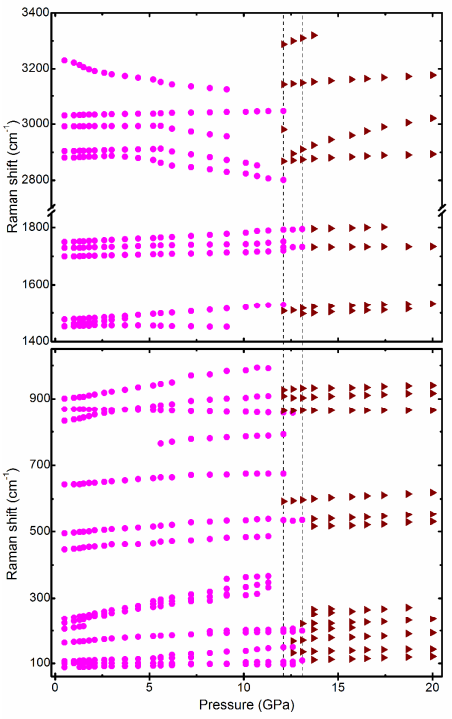

Figure S7. Frequency shift of the Raman modes as a function of pressure. The vertical dashed line marks the region of discontinuity.

As discussed by Adilson E. Motter et al. continuous contraction of a material in the same direction of an applied tension, like NLC progress, is inherently unstable.[25] So it is unreasonable for *b*-axis to have a persistent expansion with increasing pressure in ammonium oxalate monohydrate, which verified by the computational data showed in Figure S3c. As depicted in Figure S1, the XRD measurement shows that there is a phase transition in the pressure range from 12.3 GPa to 13.3 GPa. Since there are only five broad peaks left after the phase transition, we failed to make a suitable structural refinement of the new phase, but the new pressure-induced phase can be indexed to the orthorhombic polymorphic form. To gain insight into the changes of structure under high pressure, we performed high-pressure Raman scattering measurements in the pressure range from 0.5 GPa to 20.0 GPa (80 cm^{-1}-3500 cm^{-1}). The external modes of organic crystals are highly sensitive to structural changes in the crystal. Figure S6a shows the pressure-dependent external Raman vibration, it can be seen that the spectral shape of the external modes noticeably changed over pressure range from 12.1 GPa to 13.1 GPa, thereby implying the phase transition. Figure S6b shows variation of the oxalate anions related modes like oxalate deformation modes (455 cm^{-1}, 494 cm^{-1}, 644 cm^{-1}), C-C stretching modes (899 cm^{-1}), O-C-O bending modes (868 cm^{-1}), C-O stretching modes or O-C-O wagging modes (1430 cm^{-1}, 1453 cm^{-1}, 1477 cm^{-1}) under high pressure, and all of these modes undergo multiple simultaneous changes which indicated by arrows and asterisks from 12.1 GPa to 13.1 GPa. So we can deduce that the conformation and local environment of oxalate cations in the ammonium oxalate monohydrate crystal dramatically changed during phase transition. As shows in figure S6c, the Raman patterns of the N-H stretching and O-H stretching before phase transition are totally different from the ones after phase transition. Generally, N-H stretching and O-H stretching indicates the condition of N−H···O hydrogen bonds and O−H···O hydrogen bonds respectively. The disappearance of original N−H modes and emerging of new N−H modes in Raman patterns suggest that there is a substantial rearrangement in the hydrogen bonding networks. A persistent expansion with increasing pressure in *b*-axis is unreasonable. With pressure increasing up to a critical pressure, hydrogen bonding interactions cannot afford the increased

free energy anymore, and then ammonium oxalate monohydrate takes place a phase transition by means of the rearrangements of hydrogen bonding networks to reduce the free energy. As the whole, all of the abruptly changes of Raman modes (Figure S6) and the discontinues in frequency shifts (Figure S7) from 12.1 to 13.1 GPa confirmed the phase transition shown in XRD experiment. We can proposed that the phase transition is attributed to the rearrangements of hydrogen-bonding networks, just like the first phase transition in ammonium squarate which have an analogue structure with ammonium oxalate monohydrate.[27]

Reference

(1) Cairns, A. B.; Goodwin, A. L. Negative Linear Compressibility *Phys. Chem. Chem. Phys.* **2015**, 10.1039/C5CP00442J

(2) Shepherd, H. J.; Palamarciuc, T.; Rosa, P.; Guionneau, P.; Molnár, G.; Létard, J.-F.; Bousseksou, A. Antagonism between Extreme Negative Linear Compression and Spin Crossover in $[Fe(dpp)_2(NCS)_2]\cdot py$. *Angew. Chem. Int. Ed.* **2012,** *51*, 3910-3914.

(3) McCann, D. R.; Cartz, L.; Schmunk, R. E.; Harker, Y. D. Compressibility of Hexagonal Selenium by X-Ray and Neutron Diffraction. *J. Appl. Phys.* **1972,** *43*, 1432-1436.

(4) Munn, R. W. Role of the Elastic Constants in Negative Thermal Expansion of Axial Solids. *J. Phys. C: Solid State Phys.* **1972,** *5*, 535-542.

(5) Akbarzadeh, H.; Clark, S. J.; Ackland, G. J. A Theoretical Study of Selenium I under High Pressure. *J. Phys.: Condens. Matter.* **1993,** *5*, 8065-8074.

(6) Mariathasan, J. W. E.; Finger, L. W.; Hazen, R. M. High-pressure Behavior of $LaNbO_4$. *Acta Crystallogr., Sect. B* **1985,** *41*, 179-184.

(7) Kremer, R.; Loa, I.; Razavi, F.; Syassen, K. Effect of Pressure on the Magnetic Phase Transition in α'-NaV_2O_5. *Solid State Commun.* **1999,** *113*, 217-220.

(8) Haines, J.; Chateau, C.; Léger, J. M.; Bogicevic, C.; Hull, S.; Klug, D. D.; Tse, J. S. Collapsing Cristobalitelike Structures in Silica Analogues at High Pressure. *Phys. Rev. Lett.* **2003,** *91*, 015503.

(9) Goodwin, A. L.; Keen, D. A.; Tucker, M. G. Large Negative Linear Compressibility of $Ag_3[Co(CN)_6]$. *Proc. Natl. Acad. Sci. U. S. A.* **2008,** *105*, 18708-18713.

(10) Cairns, A. B.; Thompson, A. L.; Tucker, M. G.; Haines, J.; Goodwin, A. L. Rational Design of Materials with Extreme Negative Compressibility: Selective Soft-mode Frustration in $KMn[Ag(CN)_2]_3$. *J. Am. Chem. Soc.* **2011,** *134*, 4454-4456.

(11) Cairns, A. B.; Catafesta, J.; Levelut, C.; Rouquette, J.; Van Der Lee, A.; Peters, L.; Thompson, A. L.; Dmitriev, V.; Haines, J.; Goodwin, A. L. Giant Negative Linear Compressibility in Zinc Dicyanoaurate. *Nat. Mater.* **2013,** *12*, 212-216.

(12) Hodgson, S. A.; Adamson, J.; Hunt, S. J.; Cliffe, M. J.; Cairns, A. B.; Thompson, A. L.; Tucker, M. G.; Funnell, N. P.; Goodwin, A. L. Negative Area Compressibility in Silver (I) Tricyanomethanide. *Chem. Commun.* **2014,** *50*, 5264-5266.

(13) Li, W.; Probert, M. R.; Kosa, M.; Bennett, T. D.; Thirumurugan, A.; Burwood, R. P.; Parinello, M.; Howard, J. A.; Cheetham, A. K. Negative Linear Compressibility of a Metal–organic Framework. *J. Am. Chem. Soc.* **2012,** *134*, 11940-11943.

(14) Ogborn, J. M.; Collings, I. E.; Moggach, S. A.; Thompson, A. L.; Goodwin, A. L. Supramolecular Mechanics in a Metal–organic Framework. *Chem. Sci.* **2012,** *3*,

3011-3017.

(15) Serra-Crespo, P.; Dikhtiarenko, A.; Stavitski, E.; Juan-Alcañiz, J.; Kapteijn, F.; Coudert, F.-X.; Gascon, J. Experimental Evidence of Negative Linear Compressibility in the MIL-53 Metal–organic Framework Family. *CrystEngComm* **2015,** *17*, 276-280.

(16) Woodall, C. H.; Beavers, C. M.; Christensen, J.; Hatcher, L. E.; Intissar, M.; Parlett, A.; Teat, S. J.; Reber, C.; Raithby, P. R. Hingeless Negative Linear Compression in the Mechanochromic Gold Complex [$(C_6F_5Au)_2$(μ-1,4-diisocyanobenzene)]. *Angew. Chem. Int. Ed.* **2013,** *52*, 9691-9694.

(17) Fortes, A. D.; Suard, E.; Knight, K. S. Negative Linear Compressibility and Massive AnisotropicThermal Expansion in Methanol Monohydrate. *Science* **2011,** *331*, 742-746.

(18) Kamali, K.; Ravi, C.; Ravindran, T.; Sarguna, R.; Sairam, T.; Kaur, G. Linear Compressibility and Thermal Expansion of KMn [Ag (CN) $_2$] $_3$ Studied by Raman Spectroscopy and First-Principles Calculations. *J. Phys. Chem. C* **2013,** *117*, 25704-25713.

(19) Wang, K.; Duan, D.; Wang, R.; Lin, A.; Cui, Q.; Liu, B.; Cui, T.; Zou, B.; Zhang, X.; Hu, J.; Zou, G.; Mao, H. K. Stability of Hydrogen-bonded Supramolecular Architecture under High Pressure Conditions: Pressure-induced Amorphization in Melamine-boric Acid Adduct. *Langmuir* **2009,** *25*, 4787-4791.

(20) Yan, T.; Wang, K.; Tan, X.; Yang, K.; Liu, B.; Zou, B. Pressure-Induced Phase Transition in N–H···O Hydrogen-Bonded Molecular Crystal Biurea: Combined Raman Scattering and X-ray Diffraction Study. *J. Phys. Chem. C* **2014,** *118*, 15162-15168.

(21) Li, Q.; Li, S.; Wang, K.; Liu, J.; Liu, B.; Yang, K.; Zou, B. Pure Hexagonal Phase of EuF_3 Modulated by High Pressure. *J. Phys. Chem. C* **2014,** *118*, 7562-7568.

(22) Yuan, H.; Wang, K.; Wang, C.; Zhou, B.; Yang, K.; Liu, J.; Zou, B. Pressure-Induced Phase Transformations of Zircon-Type $LaVO_4$ Nanorods. *J. Phys. Chem. C* **2015,** *119*, 8364-8372.

(23) Tan, X.; Wang, K.; Yan, T.; Li, X.; Liu, J.; Yang, K.; Liu, B.; Zou, G.; Zou, B. Discovery of High-Pressure Polymorphs for a Typical Polymorphic System: Oxalyl Dihydrazide. *J. Phys. Chem. C* **2015,** *119*, 10178-10188.

(24) Frost, R. L.; Yang, J.; Ding, Z. Raman and FTIR Spectroscopy of Natural Oxalates: Implications for the Evidence of Life on Mars. *Chin. Sci. Bull.* **2003,** *48*, 1844-1852.

(25) Frost, R. L. Raman Spectroscopy of Natural Oxalates. *Anal. Chim. Acta* **2004,** *517*, 207-214.

(26) Nicolaou, Z. G.; Motter, A. E. Mechanical Metamaterials with Negative Compressibility Transitions. *Nat Mater* **2012,** *11*, 608-613.

(27) Li, S.; Wang, K.; Zhou, M.; Li, Q.; Liu, B.; Zou, G.; Zou, B. Pressure-induced Phase Transitions in Ammonium Squarate: a Supramolecular Structure Based on Hydrogen-bonding and Pi-stacking Interactions. *J Phys Chem B* **2011,** *115*, 8981-8988.